

## Influence of post-annealing temperature on double layer ZTO/GZO deposited by magnetron co-sputtering

Sung Hoon Oh<sup>a</sup>, Sang Hyun Cho<sup>a,c</sup>, Jae Heon Jung<sup>a</sup>, Sae Won Kang<sup>a</sup>, Woo Seok Cheong<sup>b</sup>, Gun Hwan Lee<sup>d</sup> and Pung Keun Song<sup>a,\*</sup>

<sup>a</sup>Department of Materials Science and Engineering, Pusan National University, Busan 609-735, Korea

<sup>b</sup>Printed Devices Research Team, ETRI, 161 Gajeong-dong, Yuseong-gu, Daejeon 305-350, Korea

<sup>c</sup>Nano Convergence Research Team, Nano Convergence Practical Application Center, Daegu Technopark, Daegu 704-801, Korea

<sup>d</sup>Functional Coatings Research Group, Korea Institute of Materials Science (KIMS), Changwon, Gyeongnam 641-831, Korea

Ga-doped ZnO (GZO) was a limit of application on the photovoltaic devices such as CIGS, CdTe and DSSC requiring high process temperature, because its electrical resistivity is unstable above 300 °C at atmosphere. Therefore, ZTO (zinc tin oxide) was introduced in order to improve permeability and thermal stability of GZO film. The resistivity of GZO (300 nm) single layer increased remarkably from  $1.8 \times 10^{-3} \Omega\text{cm}$  to  $5.5 \times 10^{-1} \Omega\text{cm}$ , when GZO was post-annealed at 400 °C in air atmosphere. In the case of the ZTO (150 nm)/GZO (150 nm) double layer, resistivity showed relatively small change from  $3.1 \times 10^{-3} \Omega\text{cm}$  (RT) to  $1.2 \times 10^{-2} \Omega\text{cm}$  (400 °C), which showed good agreement with change of carrier density. This result means that ZTO upper layer act as a barrier for oxygen at high temperature. Also ZTO (150 nm)/GZO (150 nm) double layer showed lower WVTR compared to GZO (300 nm) single layer. Because ZTO has lower WVTR compared to GZO, ZTO thin film acts as a barrier by preventing oxygen and water molecules to penetrate on top of GZO thin film.

**Key words:** ZTO, GZO, Double layer, WVTR, Solar cells, Magnetron sputtering.

### Introduction

Transparent conducting oxides (TCO) have been widely used for solar energy applications [1] and are essential components in the basic structure of many electronic devices such as flat panel displays [2], gas sensors [3] and organic light emitting diodes [4]. TCO coatings are essential for solar cell applications since they constitute a fundamental part in the emerging new generations of photovoltaic (PV) devices [5]. Indium-tin-oxide (ITO) is the most used transparent electrode material because of its high transmittance and electrical conductivity. Recently, ZnO films doped with Al, Ga or In have attracted much attention as an alternative material of ITO. Among these materials, Ga-doped ZnO (GZO) is a well-known TCO with low cost, non-toxic and high stability in hydrogen plasma compared to ITO. GZO can be easily fabricated at ambient temperature by DC magnetron sputtering on glass or plastic substrates. However, it has a limit of application on solar cell electrode such as cadmium telluride (CdTe) solar cells requiring high processing temperatures. Furthermore, a new generation of PV devices such as dye sensitized solar cells (DSSC) or organic solar cells

needs the development of new electrodes based on TCOs which must be able to keep their properties of transparency and conductivity under high temperature fabrication processes [6]. However, it was reported that the electrical resistivity of GZO is unstable above 300C in air atmosphere. This is due to absorption of oxygen at the grain boundary or exhaust of oxygen vacancy which traps carrier and reduces the mobility [7, 8].

On the other hand it was reported that amorphous ZTO(zinc tin oxide) films has high electrical stability in an air environment at 300 °C and also chemically stable in HCl and NaOH solutions [8, 9]. And also ZTO film has relatively lower permeability for oxygen and water compared to Al<sub>2</sub>O<sub>3</sub>, SiO<sub>2</sub>, TiO<sub>2</sub>, and ZnO film [10].

Therefore, this work aims to introduce ZTO thin film as a barrier layer for ZTO film in order to enhance electrical stability and water permeability. Amorphous ZTO thin film was deposited on the GZO film and then the electrical resistivity, water permeability and thermal stability for ZTO/GZO double layer were investigated in relation to the film thickness and annealing temperature.

### Experimental details

GZO thin films were prepared on non-alkali glass substrate without heating by a DC magnetron sputtering with Ga doped ZnO (Ga<sub>2</sub>O<sub>3</sub> 5.57 wt%) target. Deposition was carried out under total gas pressure of 1.0 Pa with pure Ar gas. And the target to substrate distance was

\*Corresponding author:  
Tel : +82-51-510-2390  
Fax: +82-51-512-0528  
E-mail: pksong@pusan.ac.kr

maintained at 30 mm. On the other hand, ZTO film were deposited by the co-sputtering system using two cathodes, RF and DC equipped with ZnO and SnO<sub>2</sub> target, respectively. Film thickness of GZO was adjusted to 150, 200 and 250 nm with changing deposition time at constant DC power of 70 W. Deposition of ZTO were carried out under total gas pressure of 0.5 Pa and various O<sub>2</sub> flow ratios (0.1~1.0%). Each target-substrate distance for ZnO (DC) and SnO<sub>2</sub> (RF) was 60 mm and 90 mm, respectively. Total thickness of ZTO/GZO double layer was constant with 300 nm. The microstructure of ZTO/GZO films were analyzed by X-ray diffraction (XRD, Gadds, Bruker) in continuous scan mode at a step interval of 0.022° with the X-ray generator operating at 40 kV/40 mA and field emission scanning electron microscopy (FE-SEM, Hitachi, S4700). The resistivity ( $\rho$ ), Hall mobility ( $\mu$ ) and carrier density ( $n$ ) were estimated using four-point probe and Hall effect measurements (HMS-3000, ECOPIA) using van der Pauw method. The transmittance was measured by spectrophotometer (UV-1800, Shimadzu). WVTR (water vapor transmittance rate) of the film deposited on PET substrate was estimated by Mocon (Aquatron-1).

## Results and discussion

In order to prepare high quality ZTO/GZO double layer, the optimum deposition condition of a ZTO single layer was investigated before preparation of ZTO/GZO double layer. Fig. 1(a) shows the electrical resistivity of ZTO films deposited as a function of DC power of ZnO target using pure Ar gas by co-

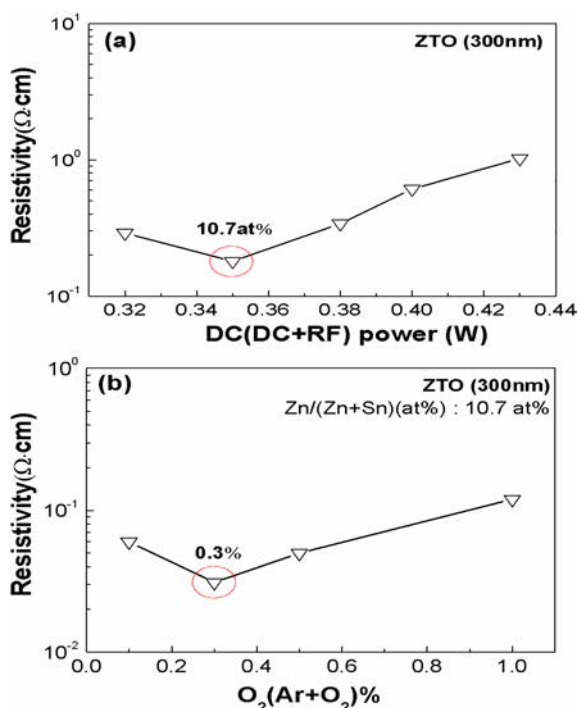


**Fig. 1.** Electrical resistivity of ZTO films deposited at various (a) Zn contents and (b) O<sub>2</sub> flow ratios.

sputtering at RF 45 W of SnO<sub>2</sub> target. The lowest resistivity of  $1.8 \times 10^{-1} \Omega\text{cm}$  is obtained for the ZTO film deposited at DC 25 W. In this case, Zn content is confirmed to be 10.7 at% Zn by EDX and then resistivity increased slightly with further increase in Zn content above 10.7 at%. However, this ZTO film did not show high transmittance in visible light region, that is, transmittance was about 73% in 550 nm. It is reported that Zn-Sn-O system has two crystal structures, the illumenite-type ZnSnO<sub>3</sub> and the inverse spinel-type Zn<sub>2</sub>SnO<sub>4</sub>, exist in the system indicating that electrical property depend on crystal structure. Zn rich Zn-Sn-O system has two phases of ZnO and Zn<sub>2</sub>SnO<sub>4</sub>. In the case of Sn rich, Zn-Sn-O system contained two phases of SnO<sub>2</sub> and ZnSnO<sub>3</sub> show lower resistivity than two phases of ZnO and Zn<sub>2</sub>SnO<sub>4</sub> [7, 11]. As a result, Zn-Sn-O system shows phase transformation from Zn<sub>2</sub>SnO<sub>4</sub> to ZnSnO<sub>3</sub> with increasing the Sn content [7, 9]. Therefore, it can be thought that low resistivity at 10.7 at% could be attributed to co-existence of ZnSnO<sub>3</sub> and SnO<sub>2</sub> two phases. By the same way, the increase of resistivity above 10.7 at% might be due to the increase of amorphous ZnO and Zn<sub>2</sub>SnO<sub>4</sub> phase contained less

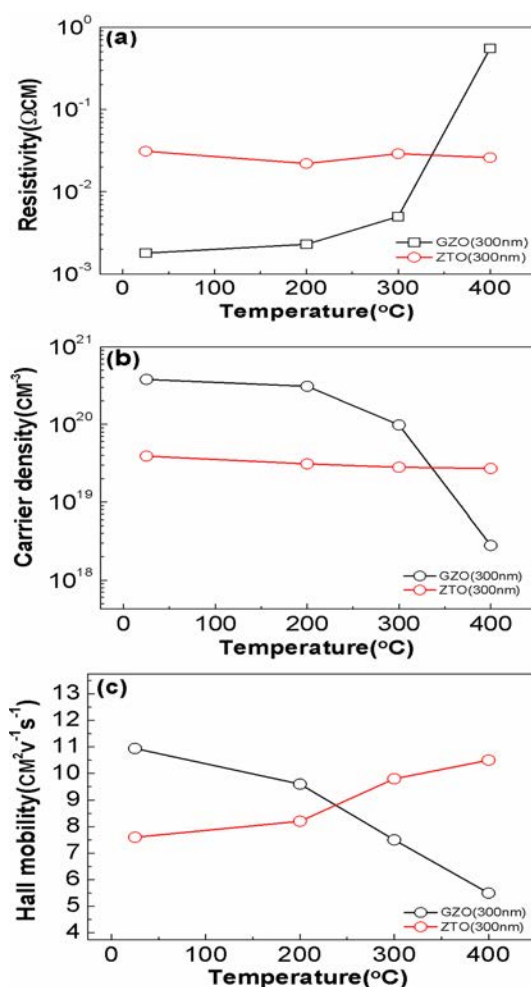


**Fig. 2.** (a) resistivity, (b) carrier density, and (c) Hall mobility of the GZO single layer and ZTO single layer deposited at different post-annealing temperatures.

oxygen vacancy in amorphous Zn-Sn-O matrix. Fig. 1 (b) shows electrical resistivity of ZTO films deposited as a function of O<sub>2</sub> flow ratio for the film contained 10.7 at% Zn. The lowest resistivity of  $3.1 \times 10^{-2} \Omega\text{cm}$  is obtained for the film deposited at O<sub>2</sub> flow ratio of 0.3%. SnO has relatively higher resistivity than SnO<sub>2</sub>. Therefore, O<sub>2</sub> introduction affect for phase transformation from nonstoichiometric SnO<sub>2-x</sub> to stoichiometric SnO<sub>2</sub>.

Fig. 2 shows the resistivity, Hall mobility and carrier concentration of the GZO and ZTO single layer with increasing annealing temperature in air atmosphere. As-deposited GZO single layer at RT showed a resistivity of  $1.8 \times 10^{-3} \Omega\text{cm}$ . However, the resistivity of the film increased slightly up to 300 °C and then increased largely at 400 °C. This large change in resistivity is mainly attributed to the decrease of carrier concentrations changed from  $3.8 \times 10^{20}$  to  $2.8 \times 10^{18} \text{cm}^{-3}$ , while the Hall mobility decreased moderately from 10.9 to 5.5 cm<sup>2</sup>/Vsec. On the other hand, the ZTO films do not show the clear increase in resistivity with

increasing annealing temperature. On the contrary, the lowest resistivity of  $2.6 \times 10^{-2} \Omega\text{cm}$  was obtained at 400 °C. The dramatic increase of the resistivity of GZO films above 300 °C has been explained by the chemisorptions of oxygen at film surfaces and grain boundaries of the film and an oxidation of interstitial Zn atoms [12]. The chemisorbed oxygen acts as trap sites of free carriers, reducing the free carriers in grains of ZnO films. And the trapped carriers cause increase of grain boundary potential barriers, leading to reduction of the Hall mobility of ZnO films [13]. On the other hand the carrier concentrations of the post-annealed ZTO film at 400 °C has changed from  $3.9 \times 10^{19}$  to  $2.7 \times 10^{18} \text{cm}^{-3}$ . This result is due to ZTO films which are very stable even in an oxidizing environment because oxygen vacancies are thought to be the major source of free carriers in ZTO films [7].

Fig. 3 shows the variation of resistivity, Hall mobility and carrier concentration of post-annealed GZO

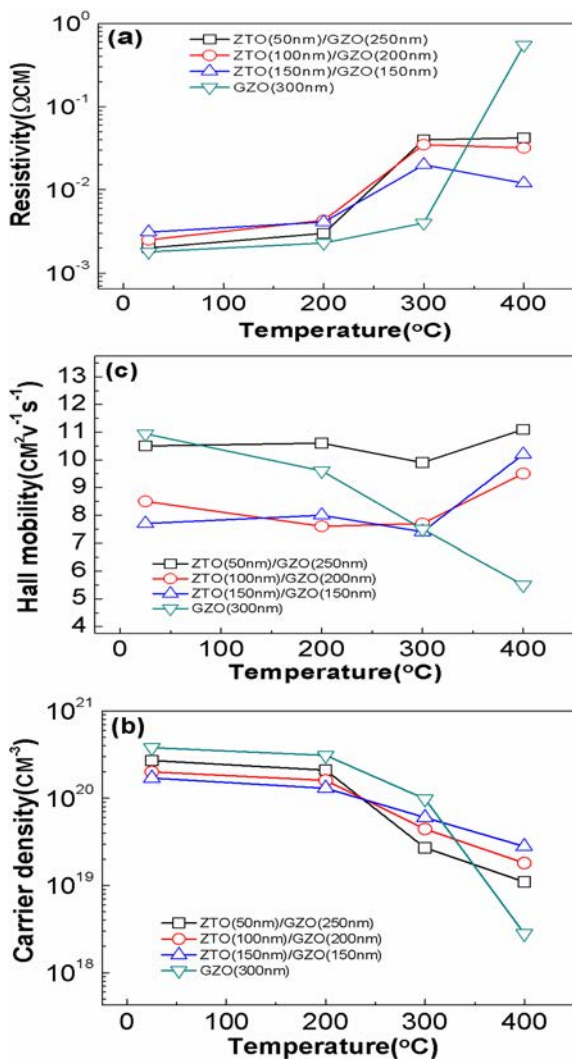


Fig. 3. (a) resistivity, (b) carrier density, and (c) Hall mobility of the ZTO/GZO double layer with different thickness under different post-annealing temperatures.

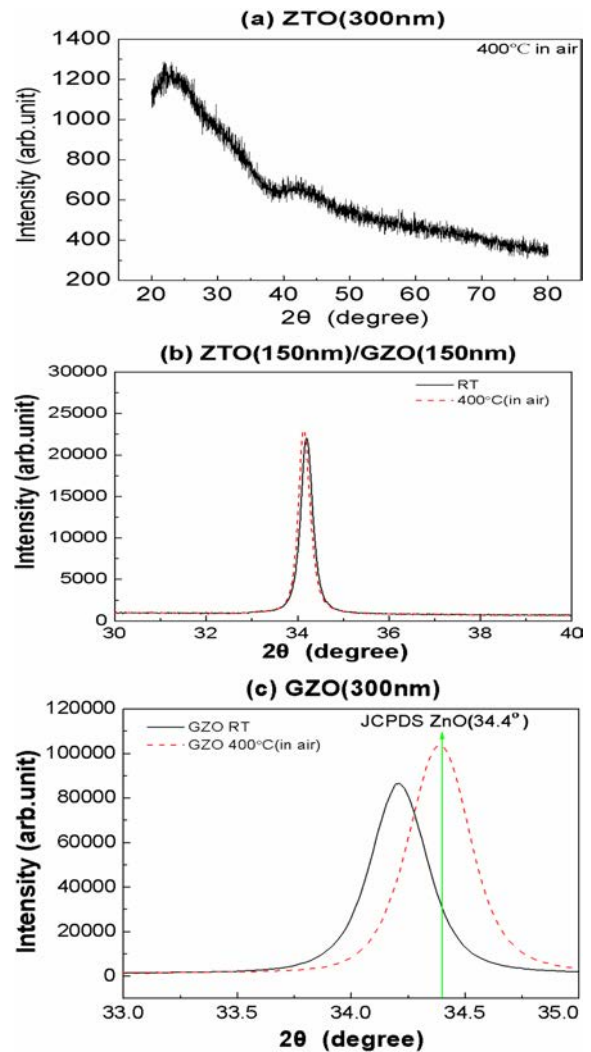
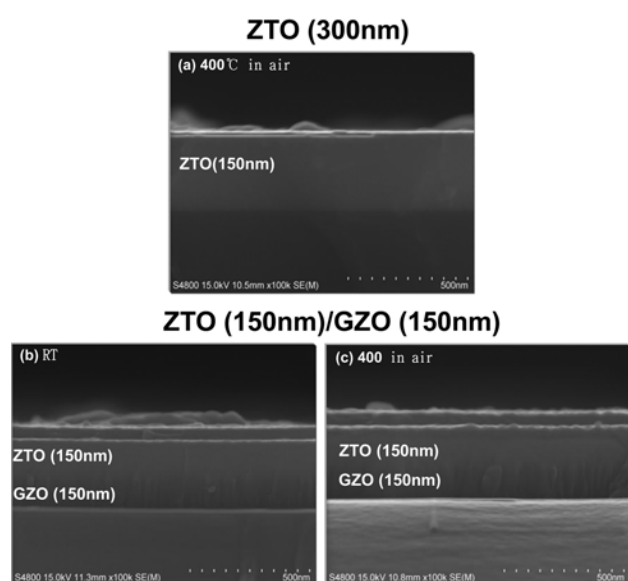


Fig. 4. XRD patterns of (a) ZTO(300 nm) single layer, (b) ZTO(150 nm)/GZO(150 nm) double layer and (c) GZO(300 nm) single layer deposited at RT and post-annealed 300 °C and 400 °C in air.



**Fig 5.** SEM cross-section images of the (a) ZTO(300 nm) single layer annealed at 400 °C in air (b) and (c) ZTO(150 nm)/GZO(150 nm) deposited RT and post- annealed at 400 °C in air.

(300 nm) and post-annealed ZTO/GZO double layer films in air. Film thickness of GZO and ZTO was adjusted as GZO (150, 200, and 250 nm) and ZTO (150, 100, and 50 nm) to fix the total film thickness 300 nm. Single GZO film (a) showed large increase in resistivity at 400 °C. However, in the case of ZTO/GZO double layer, resistivity was not changed between 300–400 °C after it showed slight increase between 200–300 °C, which showed good agreement with change of carrier density. This phenomenon is clearly observed according to increase of ZTO film thickness. Therefore, it can be said that ZTO film act effectively with barrier layer for oxygen diffusion in air.

In the case of RT, GZO single layer showed higher carrier density than ZTO/GZO double layer. However, ZTO/GZO double layer showed less decrease than GZO single layer between 300–400 °C. This phenomenon is also enhanced with increasing ZTO film thickness. On the other hand, Hall mobility of GZO single layer largely decreased with increasing annealing temperature, which could be due to absorption of oxygen at the grain boundary [13]. However, ZTO/GZO double layer showed no clear change in Hall mobility up to 300 °C. On the contrary, Hall mobility of ZTO/GZO double layer increased slightly at 400 °C. This result means that ZTO upper layer act as a barrier for oxygen at high temperature.

Fig. 4 shows XRD patterns of (a) ZTO (300 nm) film post-annealed at 400 °C in air, (b) GZO (300 nm) film as-deposited at RT and post-annealed at 400 °C in air, (c) ZTO (150 nm)/GZO (150 nm) double layer as-deposited at RT and post-annealed at 400 °C in air. Fig. 4(a) reveals that ZTO (300 nm) film maintained the amorphous structure without crystallization up to annealing temperature of 400 °C. Fig. 4(b) shows

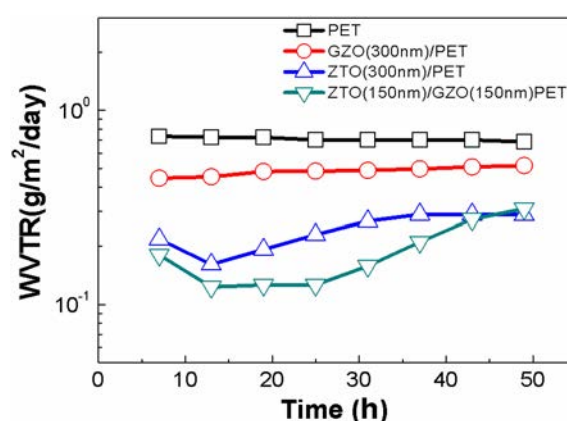


**Fig 6.** WVTR of the PET bare substrate, GZO(300 nm) single layer, ZTO(300 nm) single layer, and ZTO(150 nm)/GZO(150 nm) double layer deposited on PET substrate at RT.

preferred orientation of (002) plan of GZO layer. However, it shows no clear change in (002) peak intensity of ZTO (150 nm)/GZO (150 nm) double layer between RT and 400 °C. Fig. 4(c) GZO (300 nm) showed that (002) peak intensity increased with increasing post-annealing temperature. However, the FWHM of (002) peak was only slightly decreased at 400 °C, compared to RT. On the other hand, diffraction angle (2 theta) shifted to higher angle with increasing post-annealing temperature, that is, 2 theta was changed from 34.21 ° to 34.39 ° as post-annealing temperature increased from RT to 400 °C. The value of 34.39 ° is almost the same with JCPDS of GZO bulk (JCPDS-number: 36-, 1451). This is attributed to the decrease of internal stress caused by the thermal diffusion with increasing annealing temperature.

Fig. 5 shows the FE-SEM images of (a) ZTO single layer (300 nm) post-annealed in 400 °C at air atmosphere, (b) and (c) ZTO (150 nm)/GZO (150 nm) double layer as-deposited at RT and post-annealed at 400 °C at air atmosphere, respectively. As shown in Fig. 4(a), ZTO (300 nm) single layer is entirely amorphous structure, which shows good agreement with XRD data. In the case of Fig. 5(b), (c), it can be predicted that c-axis growth of GZO layer was interrupted by the ZTO layer.

Fig. 6 shows the WVTR (water vapor transmittance rate) in relation to time for the PET bare substrate, GZO (300 nm)/PET, ZTO (300 nm)/PET, ZTO (150 nm)/GZO (150 nm)/PET. The bare PET substrate showed the highest WVTR and in regular sequence of GZO (300 nm), ZTO (300 nm), ZTO (150 nm)/GZO (150 nm). It is thought that ZTO single layer was more suitable as a barrier layer by showing lower WVTR compared to GZO single layer. Also ZTO (150 nm)/GZO (150 nm) double layer showed lower value compared to GZO indicating that multilayer which have different crystal structure is more efficient than the single layer. Also the low WVTR result indicates that double layer surface prevent oxygen atoms and water molecules to penetrate. Because ZTO has lower WVTR compared to

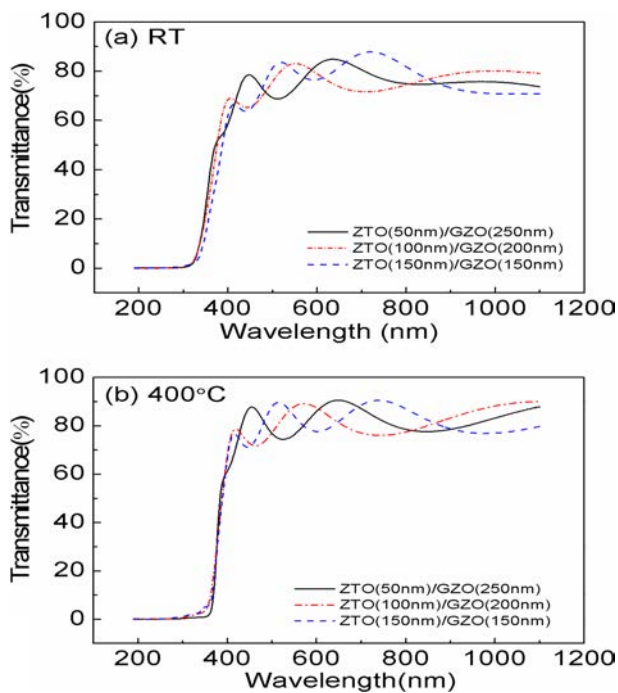


**Fig. 7.** Transmittance of (a) ZTO (50 nm)/GZO (250 nm), ZTO (100 nm)/GZO (200 nm) and ZTO (150 nm)/GZO (150 nm) deposited at RT (b) ZTO (50 nm)/GZO (250 nm), ZTO (100 nm)/GZO (200 nm), and ZTO (150 nm)/GZO (150 nm) post-annealed at 400 °C in air.

GZO, ZTO thin film acts as a barrier by preventing oxygen and water molecules to penetrate on top of GZO thin film. Also the surface of both thin film act as a barrier so when ZTO/GZO double layer is annealed in air resistivity does not increase as GZO thin film.

Fig. 7 shows the transmittance of ZTO/GZO double layer as-deposited and post-annealed at 400 °C in relation to film thickness ratio. The average transmittances of ZTO (50 nm)/GZO (250 nm), ZTO (100 nm)/GZO (200 nm), ZTO (150 nm)/GZO (150 nm) as-deposited at RT were 76, 76, and 77% in visible light region from 400 nm to 800 nm, respectively, as shown in Fig. 7(a). The average transmittances of these three types double layer increased to 81.8, 82, and 81.5%, respectively. Therefore, it can be confirmed that thickness ratio of the double layer does not affect significantly for transmittance of the films.

### Conclusion

In order to improve both electrical durability at high temperature and water permeability for GZO film, ZTO layer was introduced with upper layer. Electrical resistivity of GZO (300 nm) single layer increased remarkably from  $1.8 \times 10^{-3} \Omega\text{cm}$  to  $5.5 \times 10^{-1} \Omega\text{cm}$  as annealing temperature increased from RT to 400 °C. This dramatic increase of the resistivity due to the chemisorptions of oxygen at film surfaces and grain

boundaries of the film and an oxidation of interstitial Zn atoms. However, ZTO(150 nm)/GZO(150 nm) double layer showed good durability for high temperature in oxygen atmosphere. That is, resistivity changed from  $3.1 \times 10^{-3} \Omega\text{cm}$  (RT) to  $1.2 \times 10^{-2} \Omega\text{cm}$  (400 °C), which showed good agreement with change of carrier density. This result means that ZTO upper layer act as a barrier for oxygen at high temperature.

Also ZTO (150 nm)/GZO (150 nm) double layer showed lower WVTR compared to GZO (300 nm) single layer. Because ZTO has lower WVTR compared to GZO, ZTO thin film acts as a barrier by preventing oxygen and water molecules to penetrate on top of GZO thin film. Also the surface of both thin film act as a barrier so when ZTO/GZO double layer is annealed in air resistivity does not increase as GZO thin film.

### Acknowledgements

This research was supported in part by the human resources development of the Korea Institute of Energy Technology Evaluation and Planning (KETEP) grant funded by the Korea government, Ministry of Knowledge Economy (No. 20104010100540), and in part by R&D project of MKE/KEIT [10039263, Development of window-unified 30" touch sensor] and in part by Korea Institute of Materials Science (KIMS).

### References

1. S.H. Kim, N.M. Park, T.Y. Kim, G.Y. Sung, J. Korean Phys. Soc. 45 (2004) 676.
2. K. Ellmer, J. Phys. D, Appl. Phys. 34 (2001) 3097.
3. H. Makino, N. Yamamoto, A. Miyake, T. Yamada, Y. Hirashima, H. Iwaoka, T. Itoh, H. Hokari, H. Aoki, T. Yamamoto, Thin Solid Films 518 (2009) 1386-1389.
4. S. Takata, T. Minami, H. Nanto, Thin Solid Films 135 (1986) 183.
5. Y.H. Tak, K.B. Kim, H.G. Park, K.H. Lee, J.R. Lee, Thin Solid Films 411 (2002) 12.
6. J. Montero, C. Guillén, J. Herrero, Thin Solid Films 519 (2011) 7564-7567.
7. Y. Hayashi, K. Kondo, K. Murai, T. Moriga, I. Nakabayashi, H. Fukumoto and K. Tominaga, Vacuum 74 (2004) 607.
8. T. Minami, S. Takata, H. Sato and H. Sonohara, J. Vac. Sci. Technol. A 13(3) (1995) 1095.
9. T. Minami, H. Sonohara, S. Takata, and H. Sato, Jpn. J. Appl. Phys. 33 (1994) L1693.
10. J. Fahlteich, M. Fahland, W. Schönberger, N. Schiller, Thin solid Films 517 (2009) 3075-3080.
11. D.L. Young, H. Moutinho, Y. Yan, and T.J. Coutts, J. Appl. Phys. 92 (2002) 310.
12. J.H. Ko, I.H. Kim, D. Kim, K.S. Lee, T.S. Lee, B. Cheong, W.M. Kim, Applied Surface Science 253 (2007) 7398-7403.
13. A. Martel, F. Caballero-Briones, P. Bartolo-Perez, A. Iribarren, R. Castro Rodriguez, A. Zapata-Navarro, J.L. Pena, Surf. Coat. Technol. 148 (2001)103.